Vortex penetration in magnetic superconducting heterostructures

Serkan Erdin
School of Physics and Astronomy, University of Minnesota, 116 Church Street S.E., Minneapolis, Minnesota 55455, USA
(Received 20 January 2004; revised manuscript received 8 April 2004; published 28 June 2004)

We report our results on vortex penetration in two realizations of heterogeneos magnetic superconducting systems (HMSS) based on the London approach; semi-infinite ferromagnetic(FM)-superconducting(SC) bilayers and a FM dot on a semi-infinite SC film. In the first case, we study quantitatively the vortex entry in FM-SC bilayers which manifests Bean-Livingston-type vortex barrier, controlled by FM film's magnetization m and SC film's Ginzburg parameter κ. In the second case, we investigate the conditions for sponteneous vortex creation and determine the position of vortex for various values of magnetization and the dot's position.

DOI: 10.1103/PhysRevB.69.214521 PACS number(s): 74.25.Dw, 74.25.Ha, 74.25.Qt, 74.78.−w

I. INTRODUCTION

Heterogeneous magnetic superconducting systems (HMSS) are made of ferromagnetic (FM) and superconducting (SC) pieces separated by thin layers of insulating oxides. In contrast to the case of a homogeneous ferromagnetic superconductor studied during the last two decades, the two order parameters, the magnetization and the SC electron density do not suppress each other.[1,2] In HMSS, the strong interaction between FM and SC components stems from the magnetic fields generated by the inhomogeneous magnetization and the supercurrents as well as SC vortices. Strong interaction of the FM and SC systems not only gives rise to a new class of novel phenomena and physical effects, but also shows the important technological promise of devices whose transport properties can be easily tuned by comparatively weak magnetic fields.

Various theoretical realizations of HMSS have been proposed by different groups, such as arrays of magnetic dots on the top of a SC film,[1,3] ferromagnetic/superconducting bilayers (FSB),[4] and magnetic nanorods embedded into a superconductor,[5] whereas only submicron magnetic dots covered by thin SC films have been prepared and studied.[6–8] The experimental samples of FM-SC hybrid systems were prepared by means of electron beam lithography and lift-off techniques.[9] Both in-plane and out-of-plane magnetization was experimentally studied. The dots with magnetization parallel to the plane were fabricated from Co, Ni, Fe, Gd-Co, and Sm-Co alloys. For the dots with magnetization perpendicular to the plane which requires high anisotropy along hard-axis, Co/Pt multilayers were used.[10]

In the most of theoretical studies, the SC subsystem is considered to be an infinite size for the sake of computational simplicity. To this date, boundary and edge effects in FM-SC heterostructures have drawn very little attention,[11] though vortex entry conditions in type II superconductors have been extensively studied earlier.[12–14] However, from both the experimental and theoretical point of view, finite or semi-infinite systems are more interesting and realistic, and their study offers better understanding of vortex matter in HMSS. The author also believes that analytical and quantitative study of aforementioned systems will shed light on solving other open problems pertaining to HMSS. For example, we earlier predicted that in a finite temperature interval below the SC transition the FSB is unstable with respect to SC vortex formation in FM-SC bilayers (FSB).[15] The slow decay ($\propto 1/r$) of the long-range interactions between Pearl vortices makes the structure that consists of alternating domains with opposite magnetization and vorticity energetically favorable. It is possible that the long domain nucleation time can interfere with the observation of described textures. We also expect that domain nucleation starts near the edge, which makes qualitative study of edges in aforementioned systems necessary. Quantitative study of this dynamic process is still in progress. For this purpose, and having been motivated by current interest in HMSS, in this work, we attempt to study vortex entry conditions in HMSS. To our purpose, we work with a method based on London-Maxwell equations, which is fully explained elsewhere.[16] The London approach works well for large Ginzburg ($\kappa=\lambda_{\text{eff}}/\xi \gg 1$) parameter, where $\lambda_{\text{eff}}=\lambda_L^2/d$ is the effective penetration depth,[17] and ξ is coherence length. Indeed, for thin SC films, the Ginzburg parameter is on order of 50–100. Previously, our method was introduced for vortex structures in infinite films. Here, we extend it to semi-infinite systems. To this end, we benefit from Kogan's work on a Pearl vortex near the edge of SC thin film in which SC piece's size is considered to be semi-infinite.[18] Likewise, we consider FM subsystems on semi-infinite SC and FM subsystems in which, we assume that magnetization points perpendicular to the FM film's plane.

In this work, we first consider semi-infinite SC and FM films and study vortex entry barrier. Our calculations show that there exists Bean-Livingston-type surface barrier[19] for the vortices created by FM film. Next, we consider a circular magnetic dot near the film's edge and investigate the conditions for vortices to appear and their configurations. It turns out that, in contrast to the infinite systems, vortices are not trapped right at the dot's center, but they are shifted slightly from the center to the SC film's edge or opposite direction, depending on the dot's magnetization, position, and size. The physics behind this effect is simple. In the semi-infinite systems, the vortex interacts with both its image vortex and the magnetic dot. The competition between these two attractions determines the vortex's position. The outline of this articles is as follows: in the first section, we introduce the method to study edge effects in FM-SC systems. In the next section, we

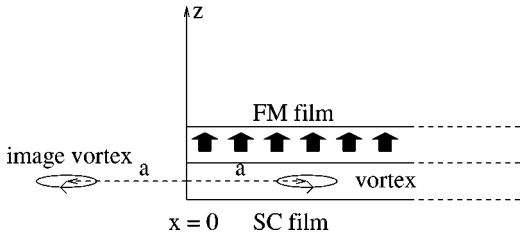

FIG. 1. Semi-infinite FM-SC bilayer.

apply our method based on Maxwell-London equations to two different cases: semi-infinite FM-SC bilayers and FM dot on a semi-infinite SC film. We conclude with results and discussions.

II. METHOD

Finite and semi-infinite systems are not as easy and straightforward as infinite systems, and they usually require more careful treatment due to the boundary of the systems. Earlier, Kogan developed a clever technique based on London approach to study a vortex near the 2D film's edge.[18] While developing our method, we stick to his technique and geometry in which a very thin SC film is located at the $x-y$ half-plane while its edge is at $x=0$ (see Fig. 1), and generalize his method for more than one vortex. We also assume that no vortex is closer to the SC film's edge than coherence length ξ, because London theory does fail in the vicinity of ξ.

We start with London equation for the vortices with vorticity n_j located at $\mathbf{r}_j$,

$$\mathbf{h}+\frac{4\pi\lambda_L^2}{c}\nabla\times\mathbf{j}_s=\phi_0\hat{z}\sum_j n_j\delta(\mathbf{r}-\mathbf{r}_j), \tag{1}$$

where $\mathbf{j}_s$ is supercurrent density in the SC subsystem. In the presence of the FM subsystem which is also considered to be very thin and located at the $x-y$ half plane as the SC subpiece, Eq. (1) turns to

$$\mathbf{h}+\frac{4\pi\lambda_L^2}{c}\nabla\times\mathbf{j}=\frac{4\pi\lambda_L^2}{c}\nabla\times\mathbf{j}_m+\phi_0\hat{z}\sum_j n_j\delta(\mathbf{r}-\mathbf{r}_j), \tag{2}$$

where $\mathbf{j}=\mathbf{j}_s+\mathbf{j}_m$ and $\mathbf{j}_m=c\nabla\times\mathbf{m}$. Averaging Eq. (2) over the thickness of the SC film, one finds

$$h_z+\frac{4\pi\lambda}{c}(\nabla\times\mathbf{g})_z=\left(\frac{4\pi\lambda}{c}\nabla\times\mathbf{g}_m\right)_z+\phi_0\sum_j n_j\delta(\mathbf{r}-\mathbf{r}_j), \tag{3}$$

where $\mathbf{g}$ is the 2D current density, which can be calculated by solving Eq. (3) together with the Biot-Savart integral equation and the continuity equation $\nabla\cdot\mathbf{g}=0$. In terms of the surface current, the Biot-Savart equation is given by

$$h_z=\frac{1}{c}\int d^2\mathbf{r}'[\mathbf{g}(\mathbf{r}')\times\mathbf{R}/R^3], \tag{4}$$

where $\mathbf{R}=\mathbf{r}-\mathbf{r}'$. Defining the surface current density in terms of a scalar function $G(\mathbf{r})$ as $\mathbf{g}=\nabla\times G(\mathbf{r})\hat{z}$, using $\mathbf{R}/R^3=\nabla'(1/R)$ and integrating Eq. (4) by parts, one can obtain

$$h_z=\frac{1}{c}\int_{x'>0} d^2\mathbf{r}'\frac{\nabla^2 G(\mathbf{r}')}{R}+\int_{-\infty}^{\infty} dy'\left(\frac{\partial_{x'}G(\mathbf{r}')}{R}\right)_{x'=0}, \tag{5}$$

where the first term gives the contribution from the entire surface current distribution whereas the second term is the contribution from the film's edge. The direct substitution of Eq. (5) into Eq. (2) gives

$$\int_{x'>0} d^2\mathbf{r}'\frac{\nabla^2 G(\mathbf{r}')}{R}+\int_{-\infty}^{\infty} dy'\left(\frac{\partial_{x'}G(\mathbf{r}')}{R}\right)_{x'=0}+4\pi\lambda\nabla^2 G(\mathbf{r})$$
$$=-c\phi_0\sum_j n_j\delta(\mathbf{r}-\mathbf{r}_j)-4\pi\lambda(\nabla\times\mathbf{g}_m)_z. \tag{6}$$

Solving the above equation in half-plane is difficult. However, this difficulty can be removed by solving (6) in the Fourier space and using the boundary conditions. That is, at the film's edge ($x=0$), the normal component of current density is zero, namely $g_x(0,y)=0$, whereas, at infinity the current distribution vanishes. This implies that the scalar function is constant at the films boundaries. For simplicity, it can be set to zero. To have G vanish at the edge, we set $G(-x,y)=-G(x,y)$. The Fourier transform of Eq. (6) reads

$$\int_0^{\infty} dx' e^{-ik_x x'}(\partial_{x'}^2-k_y^2)G(x',k_y)$$
$$+\int_{-\infty}^{\infty} dy'[\partial_{x'}G(\mathbf{r}')]_{x'=0}e^{-ik_y y'}-2\lambda k^3 G(\mathbf{k})$$
$$=i\frac{c\phi_0}{\pi}k\sum_j n_j e^{-ik_y y_j}\sin(k_x x_j)-2\lambda k(i\mathbf{k}\times\mathbf{g}_{m,k_x})_z, \tag{7}$$

where $\mathbf{k}=(k_x,k_y)$. Replacing x' by $-x'$ and writing the Eq. (7) for $-k_x$, one obtains

$$\int_0^{-\infty} dx' e^{-ik_x x'}(\partial_{x'}^2-k_y^2)G(x',k_y)$$
$$+\int_{-\infty}^{\infty} dy'[\partial_{x'}G(\mathbf{r}')]_{x'=0}e^{-ik_y y'}+2\lambda k^3 G(\mathbf{k})$$
$$=-i\frac{c\phi_0}{\pi}k\sum_j n_j e^{-ik_y y_j}\sin(k_x x_j)-2\lambda k(i\tilde{\mathbf{k}}\times\mathbf{g}_{m,-k_x})_z, \tag{8}$$

where $\tilde{\mathbf{k}}=(-k_x,k_y)$. Subtracting (8) from (7), the vortex and magnetic parts of the scalar function are found as

$$G_v(\mathbf{k})=\frac{2c\phi_0}{i\pi}\sum_j n_j\frac{e^{-ik_y y_j}\sin(k_x x_j)}{k(1+4\lambda k)}, \tag{9}$$

$$G_m(\mathbf{k})=2\lambda i\frac{[\mathbf{k}\times\mathbf{g}_{m,k_x}-\tilde{\mathbf{k}}\times\mathbf{g}_{m,-k_x}]_z}{k(1+4\lambda k)}. \tag{10}$$

Taking the inverse Fourier transform of Eq. (9), the vortex contribution in real space is found as

$$G_v(\mathbf{r}) = \frac{c\phi_0}{2\pi^2}\sum_j n_j \int_0^\infty \frac{(J_0(k|\mathbf{r}-\mathbf{r}_j|) - J_0(k|\mathbf{r}+\tilde{\mathbf{r}}_j|))}{1+4k\lambda} dk. \tag{11}$$

Note that the first term in (11) represents the jth vortex located at $\mathbf{r}_j=(x_j,y_j)$, whereas the second term is the contribution of the jth image vortex, or antivortex, at $\tilde{\mathbf{r}}_j=(-x_j,y_j)$. Next, we calculate the 2D current density. Keeping in mind that it is discontinuous at the film's edge, the Fourier components of the current density read

$$\mathbf{g}(x>0,y) = \int \frac{d^2\mathbf{k}}{(2\pi)^2}(i\mathbf{k}\times\hat{z})G(\mathbf{k})e^{i\mathbf{k}\cdot\mathbf{r}},$$

$$\mathbf{g}(x<0,y) = 0. \tag{12}$$

Using Eq. (12), one can compute vector potential and the magnetic field through

$$\mathbf{A} = \frac{4\pi}{c}\frac{\mathbf{g}}{Q^2}, \quad \mathbf{h} = \frac{4\pi}{ic}\frac{\mathbf{g}\times\mathbf{Q}}{Q^2}, \tag{13}$$

where $\mathbf{Q}=\mathbf{k}+k_z\hat{z}$. Taking the inverse Fourier of Eq. (13), the vector potential is found as

$$A_\phi(\mathbf{r}) = \frac{\phi_0}{\pi}\sum_j n_j \int_0^\infty \frac{(J_1(k|\mathbf{r}-\mathbf{r}_j|) - J_1(k|\mathbf{r}+\tilde{\mathbf{r}}_j|))e^{-k|z|}}{1+4\lambda k} dk. \tag{14}$$

At the SC film's surface ($z=0$), vector potential for one vortex with vorticity n, located at $\mathbf{r}=\mathbf{a}$ reads

$$A_\phi(\mathbf{r}) = \frac{n\phi_0}{4\lambda\pi}\left(\frac{4\lambda}{|\mathbf{r}-\mathbf{a}|} - \frac{4\lambda}{|\mathbf{r}+\tilde{\mathbf{a}}|} + \frac{\pi}{2}\left[Y_1\left(\frac{|\mathbf{r}-\mathbf{a}|}{4\lambda}\right) + H_{-1}\left(\frac{|\mathbf{r}-\mathbf{a}|}{4\lambda}\right) - Y_1\left(\frac{|\mathbf{r}+\tilde{\mathbf{a}}|}{4\lambda}\right) + H_{-1}\left(\frac{|\mathbf{r}+\tilde{\mathbf{a}}|}{4\lambda}\right)\right]\right), \tag{15}$$

where H and Y are the Struve and the second kind Bessel fuctions. At short distances ($r\ll\lambda$), A_ϕ behaves as $(n\phi_0/16\pi\lambda^2)[(-1/4+C/2-\ln 2/2)(|\mathbf{r}-\mathbf{a}|-|\mathbf{r}+\mathbf{a}|)+|\mathbf{r}-\mathbf{a}|\ln(|\mathbf{r}-\mathbf{a}|/4\lambda)-|\mathbf{r}+\mathbf{a}|\ln(|\mathbf{r}+\mathbf{a}|/4\lambda)$ whereas, at large distances, it decays slowly in space, namely $(\phi_0/\pi)(1/|\mathbf{r}-\mathbf{a}| - 1/|\mathbf{r}+\mathbf{a}|)$. $C=0.577\ldots$ is a Euler constant. Magnetic field due to the vortex in the z direction reads

$$h_z(\mathbf{r}) = \frac{n\phi_0}{\pi}\int_0^\infty \frac{(J_0(k|\mathbf{r}-\mathbf{a}|) - J_0(k|\mathbf{r}+\mathbf{a}|))ke^{-k|z|}}{1+4\lambda k} dk. \tag{16}$$

At $z=0$, the magnetic field reads

$$h_z(\mathbf{r}) = \frac{n\phi_0}{4\lambda\pi}\left(\frac{1}{|\mathbf{r}-\mathbf{a}|} - \frac{1}{|\mathbf{r}+\mathbf{a}|} - \frac{\pi}{8\lambda}\left[H_0\left(\frac{|\mathbf{r}-\mathbf{a}|}{4\lambda}\right) - Y_0\left(\frac{|\mathbf{r}-\mathbf{a}|}{4\lambda}\right) - H_0\left(\frac{|\mathbf{r}+\mathbf{a}|}{4\lambda}\right) - Y_0\left(\frac{|\mathbf{r}+\mathbf{a}|}{4\lambda}\right)\right]\right). \tag{17}$$

The asymptotics of the magnetic field at small and large distances are

$$h_z \sim \frac{n\phi_0}{4\pi\lambda}\left(\frac{1}{|\mathbf{r}-\mathbf{a}|} - \frac{1}{|\mathbf{r}+\mathbf{a}|} + \frac{1}{4\lambda}\ln\frac{|\mathbf{r}-\mathbf{a}|}{|\mathbf{r}+\mathbf{a}|}\right) \quad r\ll\lambda, \tag{18}$$

$$h_z \sim \frac{4n\lambda\phi_0}{\pi}\left(\frac{1}{|\mathbf{r}-\mathbf{a}|^3} - \frac{1}{|\mathbf{r}+\mathbf{a}|^3}\right) \quad r\gg\lambda. \tag{19}$$

The total energy of the FM-SC system reads

$$E = E_v + E_{vm} + E_m, \tag{20}$$

where E_v is the vortex energy, E_{vm} is the interaction of vortex and magnetic subsystem, and finally E_m is self-energy of the magnetic subsystem, which will be ignored at further calculations, since it is inappropriate for our problem. Vortex energy is calculated by Kogan[18] as

$$E_v = \sum_{i,j}{}' \frac{n_i\phi_0}{2c}G_v(\mathbf{r}\to\mathbf{r}_j), \tag{21}$$

where Σ' denotes the restricted sum in which only $i=j$ and $i>j$ are taken into account. Equation (21) leads to

$$E_v = \sum_i \frac{n_i^2\phi_0^2}{16\pi^2\lambda}\left[\ln\frac{8\lambda}{e^C\xi} - \frac{\pi}{2}\Phi_0\left(\frac{x_i}{2\lambda}\right)\right] + \sum_{i>j}\pi\varepsilon_0 n_i n_j\left[\Phi_0\left(\frac{\mathbf{r}_i-\mathbf{r}_j}{4\lambda}\right) - \Phi_0\left(\frac{\mathbf{r}_i+\mathbf{r}_j}{4\lambda}\right)\right], \tag{22}$$

where $\Phi_0(x)=Y_0(x)-H_0(x)$. Vortex-magnetization interaction energy is calculated as in[16]

$$E_{vm} = -\frac{\phi_0}{16\pi\lambda^2}\int \nabla\varphi\cdot\mathbf{a}^m d^2x - \frac{1}{2}\int \mathbf{m}\cdot\mathbf{b}^v d^2x, \tag{23}$$

where integration is performed over the half-space. Note that we take $\lambda/\xi=50$ in our numerical calculations.

A. Semi-infinite FM-SC bilayers

In this part, we study a semi-infinite FM film on top of a semi-infinite SC film. Both films are taken to be very thin, lie on the x–y half-plane, whereas their edges are located at $x=0$ (see Fig. 1). We assume that FM film has uniform magnetization along the z direction and has high anisotropy, so that its magnetization does not change direction due to the magnetic field of the vortex. The magnetization of the FM film reads

$$\mathbf{m} = m\theta(x)\delta(z)\hat{z}. \tag{24}$$

Magnetic current in real space and Fourier space is given as

$$\mathbf{g}_m = -mc\delta(x)\hat{y}, \quad \mathbf{g}_{m,k} = -2\pi mc\delta(k_y)\hat{k}_y. \tag{25}$$

Substituting Eq. (24) into Eq. (10), one can find the scalar potential as

$$G_m(\mathbf{k}) = -8\pi\lambda mci\frac{k_x\delta(k_y)}{k(1+4\lambda k)}. \tag{26}$$

Taking the inverse Fourier transform of Eq. (26) we find

$$G_m(x) = \frac{mc}{\pi}f\left(\frac{x}{4\lambda}\right), \tag{27}$$

where $f(x)=\int_0^\infty dk_x \sin(k_x x)/(1+k_x)$. The asymptotics of $f(x)$ are

$$f(x) \approx \frac{\pi}{2} + x(\ln(x) + C - 1), x \ll 1, \tag{28}$$

$$f(x) \approx \frac{1}{x}, x \gg 1.$$

Using Eq. (12) and (13), the z component of the screened magnetic field at $z=0$ due to the FM film, reads

$$h_z(\mathbf{r}) = \frac{m}{4\lambda}\int_0^\infty \frac{k_x \sin\left(k_x\frac{x}{4\lambda}\right)}{1+|k_x|}dk_x. \tag{29}$$

The magnetic field decays as $1/x$ for $x \ll \lambda$ and $1/x^2$ for $x \gg \lambda$. In order to study vortex configuration, we need to calculate total effective energy of the system. To this end, we consider a simple case, namely a vortex with a single flux located at $\mathbf{r}=\mathbf{a}$. For this case, vortex energy for a single vortex reads [see Eq. (22)]

$$E_v = \frac{\phi_0^2}{16\pi^2\lambda}\left[\ln\frac{8\lambda}{e^\lambda\xi} - \frac{\pi}{2}\Phi_0\left(\frac{a}{2\lambda}\right)\right], \tag{30}$$

wheras the vortex-magnetization interaction energy can be calculated by means of Eq. (23),

$$E_{vm} = -m\phi_0\left[1 - \frac{2}{\pi}f\left(\frac{a}{4\lambda}\right)\right]. \tag{31}$$

The sum of Eqs. (22) and (31) gives the effective total energy of the system. Vortex becomes energetically favorable when effective total energy becomes less than zero. Equating the effective energy to zero, one can obtain the curve for spontenous creation of the vortex. This curve,

$$\frac{m\phi_0}{\varepsilon_0} = \frac{\ln\left(\frac{8\lambda}{e^\lambda\xi}\right) - \frac{\pi}{2}\left(H_0\left(\frac{a}{2\lambda}\right) - Y_0\left(\frac{a}{2\lambda}\right)\right)}{1 - \frac{2}{\pi}f\left(\frac{a}{4\lambda}\right)} \tag{32}$$

separates the regions where the vortex appears spontaneously and does appear as seen in Fig. 2. For large values of the $m\phi_0/\varepsilon_0$ ratio, the vortex comes out near the edge. On the other hand, it prefers going further away from the surface for a small ratio of $m\phi_0/\varepsilon_0$. We can estimate the minimum value of magnetization of the FM film through effective energy for

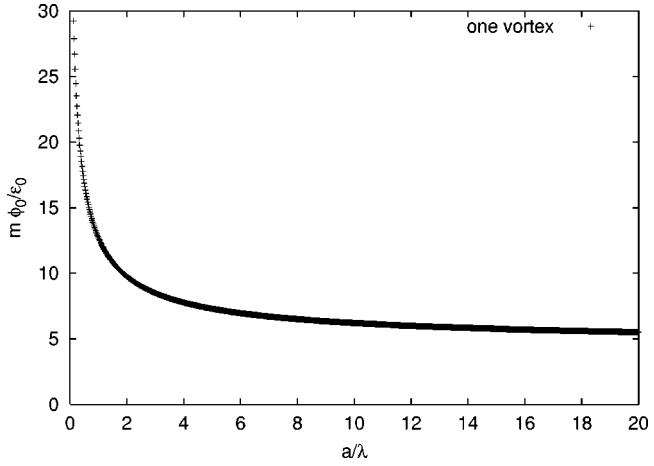

FIG. 2. Phase diagram of a single vortex created by the semi-infinite FM film. In the region below the curve, the vortex does not appear, whereas it becomes energetically favorable in an area above the curve.

infinite films,[16] which is $E_{\text{eff}}=\varepsilon_0\ln(\lambda/\xi)-m\phi_0$. Equating this equation to zero and solving it for m, we find $m_{c1}=\phi_0/(16\pi^2\lambda\ln(\lambda/\xi))$. When magnetization exceeds this value, the vortex appears very far away from the edge. In order to get the vortex to appear close to the edge, m must be significantly larger than m_{c1}. Another interesting thing is that the system manifests a Bean-type surface barrier for the vortex. The surface barrier is controlled by $m\phi_0/\varepsilon_0$ and Ginzburg parameter κ. We analyze three regimes for this ratio for fixed $\kappa=\lambda/\xi$. When $m<m_{c1}$, vortex does not appear (see Fig. 3). In the second regime, $m_{c1}<m<m_{c2}$, vortex prefers going further away from the surface, whereas, when $m>m_{c2}$, the barrier disappears (see Fig. 4). m_{c2} is the second critical magnetization, at which barrier disappears, and can be calculated through the condition that the slope $|\partial E_{\text{tot}}/\partial x|_{x=\xi}$ is zero, which gives $m\phi_0/\varepsilon_0 \approx 2\pi\kappa/\ln(4\kappa)$. When ratio $m\phi_0/\varepsilon_0$ is greater than this, the barrier disappears. Physically, two contributions play an important role for the vortex barrier. Namely, the vortex is attracted to the SC film's edge through its attraction towards image vortex whereas it is re-

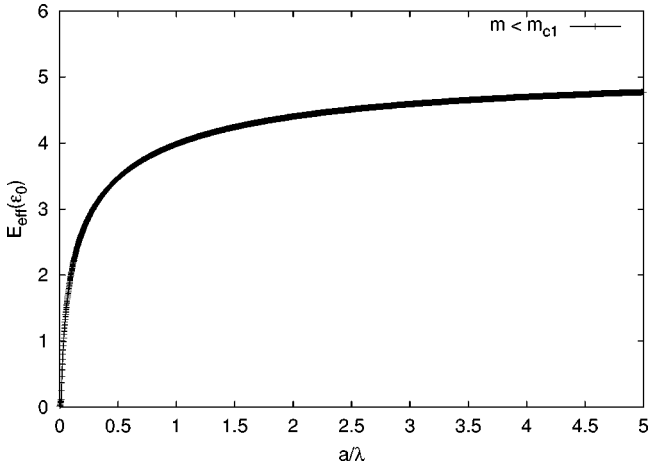

FIG. 3. The effective energy versus the vortex's position. When $m<m_{c1}$, the vortex does not appear.

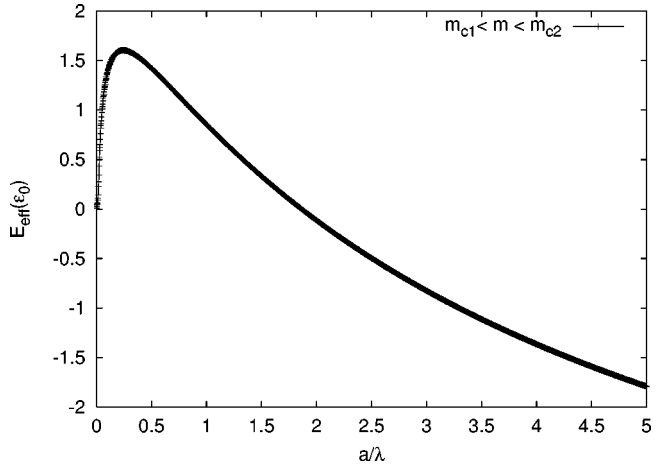

FIG. 4. The effective energy versus the vortex's position. When $m_{c1}<m<m_{c2}$, the surface barrier shrinks toward the edge of the SC film, and the vortex is created a little further from the edge.

pelled by the FM film's edge. Competition between these two factors controls the barrier (see Fig. 5).

B. FM dot on a semi-infinite SC film

In this case, we study a circular FM disc on top of semi-infinite SC film. Earlier, we studied the conditions for the vortex states to appear on a similar system, in which SC film, however was infinite. Due to the circular symmetry of the FM dot, vortex was appearing at the dot's center. In this section, we study the vortex states in more realastic case and investigate the role of edge effects on the spontaneous formation of the vortex due to the FM dot. To this end, we start with the magnetization of a circular FM disc located at $\mathbf{r}_d=(x_d,0)$,

$$\mathbf{m}=m\theta(R-|\mathbf{r}-\mathbf{r}_d|)\,\delta(z)\hat{z}, \tag{33}$$

where R is the radius of the circular dot. The Fourier transform of Eq. (33) reads

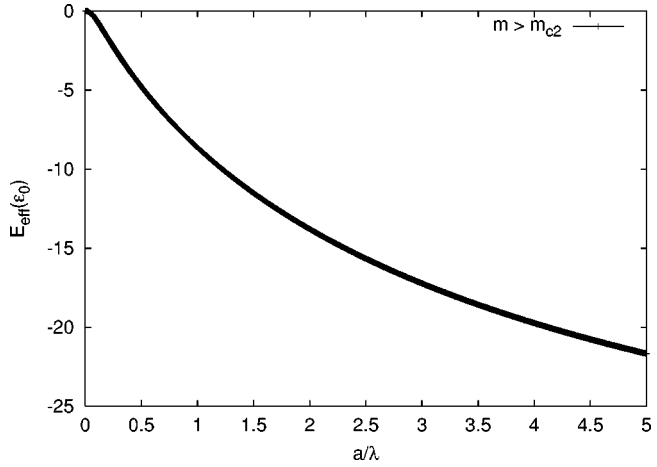

FIG. 5. The effective energy versus the vortex's position. When $m>m_{c2}$ the barrier disappears, and the vortex can be seen anywhere in the SC film.

TABLE I. The position of vortices for different values of the r_d/λ, R/λ, and $m\phi_0/\epsilon_0$. The two columns on the left are input.

r_d/λ	R/λ	a/λ	$m\phi_0/\epsilon_0$
2.0	2.0	2.04	17
2.0	2.0	2.32	187
3.0	3.0	3.12	31
3.0	3.0	3.44	132
4.0	4.0	4.20	11
4.0	4.0	4.56	185

$$\mathbf{m}_\mathbf{k}=2\pi mR\frac{J_1(kR)e^{-ik_x x_d}}{k}. \tag{34}$$

Using Eqs. (10), (12), and (13) together with Eq. (34), one can calculate the screened magnetic field due to the FM dot as

$$h_z(r,z)=4\pi m\lambda R\times\int_0^\infty\frac{J_1(kR)[J_0(k|\mathbf{r}-\mathbf{r}_d|)-J_0(k|\mathbf{r}+\mathbf{r}_d|)]k^2e^{-k|z|}}{1+4\lambda k}dk. \tag{35}$$

Outside the dot, magnetic field decays rapidly in space, namely, for $r\ll\lambda$, $\sim 1/r^3$, whereas for $r\ll\lambda$, $\sim 1/r^5$. From Eq. (23), the vortex-magnetic disc interaction energy reads

$$E_{vm}=-m\phi_0R\int_0^\infty J_1(kR)\frac{[J_0(k|\mathbf{r}_d-\mathbf{a}|)-J_0(k|\mathbf{r}_d+\mathbf{a}|)]}{1+4\lambda k}dk. \tag{36}$$

After we formulate the total effective energy as $E=E_v+E_{vm}$, where E_v is given in Eq. (30), we study the conditions for a vortex to appear spontaneously. The criteria for spontaneous vortex formation is that effective energy becomes negative. However, vortex in semi-infinite systems also interacts with its image. Therefore, it is necessary to minimize total effective energy with respect to the vortex position. To this end, we first fix the dot's location and value of $m\phi_0/\varepsilon_0$ and vary the vortex's position afterwards, to find the minimum total effective energy. In our calculations, we investigate where vortex first comes out, and how it is shifted with a further increase of $m\phi_0/\varepsilon_0$. For this purpose, we determine the vortex's position for different values of the r_d/λ, R/λ, and $m\phi_0/\varepsilon_0$, by optimizing the total effective energy. Our results are shown in Table I and Fig. 6.

According to our calculations, vortex appears first close to the edge except $r_d/R\geqslant 10$ case, in which it sits at the dot's center. On the other hand, when $m\phi_0/\varepsilon_0$ is increased further, vortex is first shifted towards the dot's center. With further increase of $m\phi_0/\varepsilon_0$, it drifts away from the dot's center. However, this is not always the general picture. In the case of $r_d/R>5/3$, vortex is located at the dot's center even for large values of $m\phi_0/\varepsilon_0$. However, for larger dot's sizes ($r_d/R\sim 1$ and $r_d/\lambda\geqslant 2$) vortex first appears away from the dot's center. This situation differs from the vortex in an infi-

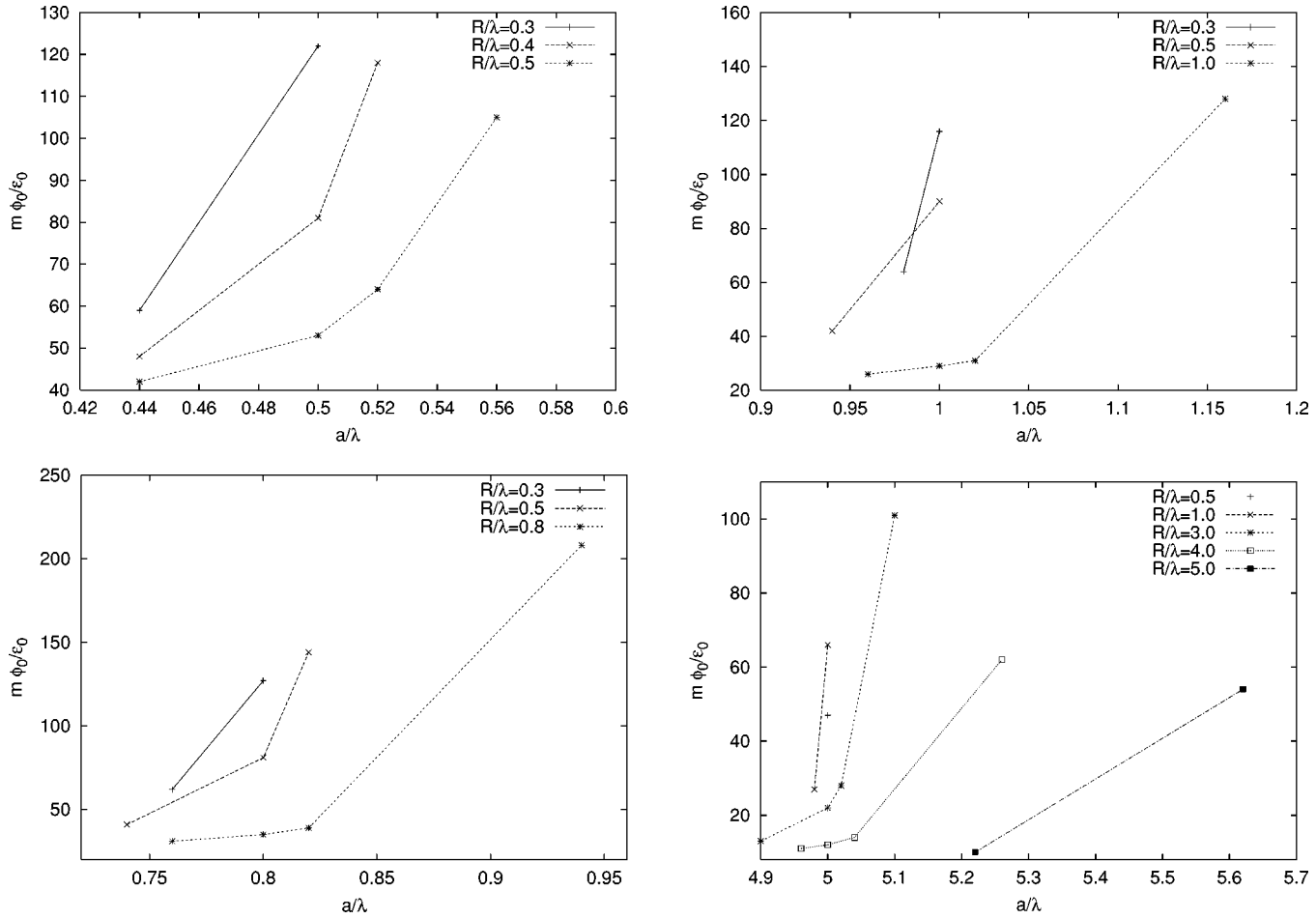

FIG. 6. Position of the vortex a/λ versus $m\phi_0/\varepsilon_0$ for various locations r_d/λ and sizes R/λ of the magnetic dot.

nite system. In the latter, only the force acting on the vortex stems from the vortex-magnetization interaction, and due to the dot's circular symmetry, it comes out at the dot's center. However, in this case, there is another force coming from the vortex-image vortex, which decays slowly $\sim 1/r$ for large distances $r > \lambda$ and pulls the vortex towards the SC film's edge, whereas the force exerted by the magnetic dot pushes the vortex towards the dot's center. As a result, the vortex's position is determined by the balance between these two forces.

III. CONCLUSIONS

In this article, we studied vortex entry conditiions in HMSS. First, we generalized Kogan's method for quantitative study of semi-infinite HMSS. For applications, we first considered semi-infinite FM film on top of a semi-infinite SC film. The quantative analysis of this system showed that the vortex undergoes Bean-type barrier which is controlled by two intrinsic properties of the system; FM film's magnetization m and Ginzburg parameter κ. Note that our result is valid only for a single flux. Our study for the case of several fluxes will be published elsewhere. Secondly, we studied a single circular FM dot on a semi-infinite SC film. We analyzed the conditions for sponteneous vortex creation and vortex location for various positions of the dot. It turns out that the vortex does not always appear at the dot's center, which differs from the case in which there is a similar dot on an infinite SC film. In closing, there are two important contributions in semi-infinite HMSS: attraction of vortex to the edge through its image vortex and vortex-magnetization interaction. As a result of competion betweeen these two factors, peculiar physical effects which do not come out in infinite HMSS, appear. In this work, we studied the simplest cases to get an idea about edge effects in HMSS. However, there are still several interesting realizations that can be studied via the method that is developed here. We leave them for possible future works.

[1] I. F. Lyuksyutov and V. L. Pokrovsky, Phys. Rev. Lett. **81**, 2344 (1998).
[2] I. F. Lyuksyutov and V. L. Pokrovsky, Proc. SPIE **3480**, 230 (1998).
[3] S. Erdin, Physica C **391**, 140 (2003).
[4] I. F. Lyuksyutov and V. L. Pokrovsky, cond-mat/9903312 (unpublished).
[5] I. F. Lyuksyutov and D. G. Naugle, Mod. Phys. Lett. B **13**, 491 (1999).
[6] J. I. Martin, M. Velez, J. Nogues, and I. K. Schuller, Phys. Rev. Lett. **79**, 1929 (1997).
[7] D. J. Morgan and J. B. Ketterson, Phys. Rev. Lett. **80**, 3614 (1998).
[8] Y. Otani, B. Pannetier, J. P. Nozieres, and D. Givord, J. Magn. Magn. Mater. **126**, 622 (1993).
[9] M. J. Van Bael, K. Temst, V. V. Moshchalkov, and Y. Bruynseraede, Phys. Rev. B **59**, 14674 (1999).
[10] M. J. Bael, L. Van Look, K. Temst *et al.*, Physica C **332**, 12 (2000).
[11] Yu. A. Genenko, and S. V. Yampolskii, cond-mat/0311157 (unpublished).
[12] P. G. de Gennes, Solid State Commun. **3**, 127 (1965).
[13] L. Kramer, Phys. Rev. **170**, 475 (1968).
[14] D. Y. Vodolazov, I. L. Maksimov, and E. H. Brandt, Physica C **384**, 211 (2003).
[15] S. Erdin, I. F. Lyuksyutov, V. L. Pokrovsky, and V. M. Vinokur, Phys. Rev. Lett. **88**, 017001 (2002).
[16] S. Erdin, A. M. Kayali, I. F. Lyuksyutov, and V. L. Pokrovsky, Phys. Rev. B **66**, 014414 (2002).
[17] A. A. Abrikosov, *Introduction to the Theory of Metals* (North-Holland, Amsterdam, 1986).
[18] V. G. Kogan, Phys. Rev. B **49**, 15874 (1994).
[19] C. P. Bean and J. D. Livingstone, Phys. Rev. Lett. **12**, 14 (1964).